# Electrically Tunable Selective Light Absorber using Epsilon-Near-Zero InSb and High-k Dielectrics


1$^{st}$ Soham Chatterjee
*Department of Physics*
*IIT Guwahati, India*
chsoham04@gmail.com

2$^{nd}$ Rajib Lochan Ghadei
*Department of Physics*
*IIT Guwahati, India*
rajiblochanghadei@gmail.com

3$^{rd}$ Rishi Maiti*
*Department of Physics*
*IIT Guwahati, India*
rmaiti@iitg.ac.in



***Abstract*—This paper presents a comprehensive numerical investigation of an electrically tunable selective light absorber. The device architecture is a Fabry-Perot nanocavity employing an n-doped Indium Antimonide (InSb) thin film as an Epsilon-Near-Zero (ENZ) active medium. Electrical gating results in a dynamical shift of the ENZ wavelength of InSb to modulate the device's reflectance. We utilize a multi-physics simulation framework, coupling the Ansys CHARGE solver for electrostatic analysis with a Transfer Matrix Method (TMM) model to compute the reflectance spectra calculations. A comparative analysis of three high-k gate dielectrics: Titanium dioxide ($TiO_2$), Hafnium dioxide ($HfO_2$), and Zirconium dioxide ($ZrO_2$) is performed to identify the optimal material for maximizing absorption and corresponding spectral shift, demonstrating a viable path toward efficient, CMOS compatible optical devices. The absorption wavelength is controlled not only by electrical gating but also by varying the insulator material and tailoring the thickness of the nanocavity. An appropriate increase in the cavity region thickness resulted in a shift in resonant wavelength from visible to near infrared region. With judicious material selection and appropriate biasing, the device achieves a 40 nm spectral shift in the visible range, reaching a reflectance dip of 97.6%, while in the near-infrared it exhibits a larger 115 nm shift accompanied by a dip of 73.7%, making it promising for tunable photonic applications.**



***Index Terms*—Epsilon-Near-Zero (ENZ), Indium Antimonide (InSb), High-k dielectrics, Electrically tunable light Absorber, Fabry-Perot nanocavity, Transfer Matrix Method.**


## I. INTRODUCTION

There has been significant progress in the design of spectrally selective light absorbers which find use in a wide range of applications such as color filters, biological and chemical sensing etc. However, conventional optical elements are usually functionally static, limiting their adaptability to dynamic environments. Thus there is rising demand for dynamic photonic components which is driving modern research into electrically reconfigurable devices, which offer high speed operation and seamless integration with CMOS electronics [1] [2]. Epsilon-Near-Zero (ENZ) materials are characterized by the fact that the real part of their dielectric permittivity ($Re\{\epsilon\}$ tends to 0) vanishes at a specific frequency, thus providing a powerful platform for such devices [3]. The high sensitivity of the refractive index to permittivity changes near the ENZ point makes these materials ideal for dynamic modulation . By electrically altering a material's carrier concentration, its ENZ condition can be spectrally shifted, enabling significant control over its optical properties. While transparent conducting oxides (TCOs) are common for near-infrared applications, n-doped Indium Antimonide (InSb) is a compelling alternative for both visible and near IR range [4]. InSb's narrow bandgap (∼0.17 eV), high intrinsic carrier concentration and high electron mobility are highly advantageous. According to the Drude model, the plasma frequency ($\omega_p$) is proportional to $\sqrt{N/m^*}$. The small effective mass in InSb places its plasma frequency naturally in the infrared, making its ENZ point highly tunable via carrier density modulation [5].

In this work, we theoretically investigate an electrically tunable selective light absorber based on an n-InSb fabry-perot nanostructure. The application of a gate voltage leads to the accumulation of majority charge carriers near the semiconductor insulator interface, modifying the local permittivity and consequently the spectral response of the device [6]. The novelty of our study is a systematic comparison of three high-k dielectrics ($TiO_2$, $HfO_2$, and $ZrO_2$) as the insulator. High-k materials are chosen to maximize gate capacitance, thereby enhancing the field effect carrier modulation and improving absorber performance. Varying the insulator materials leads to a variance in the resonant wavelengths. It is also noted that by varying the thickness of the cavity region, the selective absorption wavelength along with the tunable spectral shift can be significantly modulated.

## II. STRUCTURE AND COMPUTATIONAL DETAILS

### A. Device Architecture

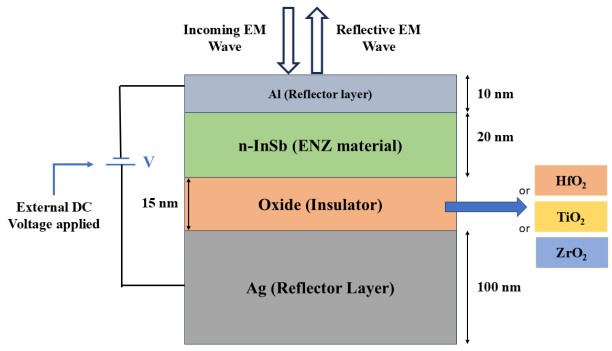


Fig. 1. Schematic of electrically tunable light absorber.

The proposed structure is designed as a Fabry-Perot nanocavity, comprising a top reflector layer of aluminum (Al)

with a thickness of 10 nm and a bottom substrate layer of gold (Au) with a thickness of 100 nm. The active region of the cavity is formed by a 20 nm thick semiconductor layer of n-doped indium antimonide (n-InSb), which exhibits ENZ epsilon-near-zero (ENZ) characteristics. This semiconductor layer is followed by a 20 nm thick insulating layer, where the dielectric material is varied among three high-k oxides: hafnium dioxide ($HfO_2$), titanium dioxide ($TiO_2$), and zirconium dioxide ($ZrO_2$). Electric gating is applied to the structure by grounding the top metal contact of aluminum and applying a Voltage Bias of 0V and 15V to the bottom metal contact of silver.

### *B. Simulation Methodology*

A multi-physics workflow was employed to model the device's electro-optical response. First, the depth-dependent electron concentration profile, N(z), was calculated under bias by solving the Poisson and drift-diffusion equations using the Ansys CHARGE solver [7] . This charge profile then determined the local complex permittivity of the InSb layer via the Drude model, allowing the total optical reflectance to be computed using the Transfer Matrix Method (TMM). The CHARGE solver utilizes material parameters from its built-in library, which includes the work functions of 5.1 eV for Ag and 4.28 eV for Al and relative dielectric permittivities of 25, 80 and 24 for $HfO_2$ , $TiO_2$ and $ZrO_2$ respectively. For the semiconductor InSb, the solver uses a DC permittivity of 16.8, work function of 4.71 eV, effective mass of 0.023 $m_e$ and intrinsic carrier density of 1.92 × $10^{16}$ $cm^{-3}$. The doping tool was set to n-type doping with constant concentrations of 3.5 × $10^{17}$ $cm^{-3}$, applied to the semiconductor layer. At zero applied voltage, the carrier density of n-InSb is $N = 3.5 \times 10^{17}\,\mathrm{cm}^{-3}$. Applying a voltage of 15V to the bottom Ag layer creates an accumulation layer in the n-InSb near the semiconductor-insulator interface, increasing the electron density to approximately $N = 2.68 \times 10^{22}\,\mathrm{cm}^{-3}$. The dielectric constant and refractive index of n-InSb films at carrier densities $N_1 = 3.5 \times 10^{17}\,\mathrm{cm}^{-3}$ and $N_2 = 2.68 \times 10^{22}\,\mathrm{cm}^{-3}$ are determined using the Drude model. For zero voltage ($N_1$), the ENZ wavelength occurs in the infrared at $35.17\,\mu\mathrm{m}$; when $15\,\mathrm{V}$ is applied, the electron density reaches $N_2$, shifting $\lambda_{\mathrm{ENZ}}$ to $126\,\mathrm{nm}$ in the visible spectrum. The optical parameters for Ag and Al, and the insulators ($HfO_2$, $TiO_2$ and $ZrO_2$) were taken from Palik [8]

TABLE I
DRUDE PARAMETERS FOR INSB (*near interface data*)

| **Electric Gating** | $\epsilon_\infty$ | **N ($cm^{-3}$)** | $\omega_p$ **(rad/s)** | $\gamma$ **(rad/s)** | **ENZ** $\lambda$ **($\mu$m)** |
|---|---|---|---|---|---|
| 0 V | 16.8 | $3.5 \times 10^{17}$ | $2.20 \times 10^{14}$ | $2.1 \times 10^{12}$ | 35.17 |
| 15 V | 16.8 | $2.68 \times 10^{22}$ | $6.089 \times 10^{16}$ | $2.351 \times 10^{12}$ | 0.126 |

## III. THEORY

Ansys Charge Solver solves drift and diffusion equations along with Poisson's equations which leads to the equation:

$$N(z) = N_0 e^{q\psi(z)/kT} \tag{1}$$

Equation (1) gives an expression of N as a function of z and $\psi$(z) where z is the distance from semiconductor-insulator interface with z = 0 at interface [9]. k denotes Boltzmann constant and T is the temperature. $\psi$(z) denotes the electrostatic potential as a function of z.

Next, the optical properties of n-InSb are described by the Drude model, which relates the complex dielectric permittivity $\epsilon(\omega)$ to the free electron dynamics as given below [10]:

$$\varepsilon = \varepsilon' - j\varepsilon'' \qquad n = \sqrt{\varepsilon} \tag{2}$$

$$\varepsilon' = \varepsilon_\infty - \frac{\omega_p^2}{\omega^2 + \gamma^2} \qquad \varepsilon'' = \frac{\gamma\omega_p^2}{\omega(\omega^2 + \gamma^2)} \tag{3}$$

$$\omega_p = \sqrt{\frac{Ne^2}{m^*\varepsilon_0}} \qquad \omega_{\mathrm{ENZ}} = \sqrt{\frac{\omega_p^2 - \varepsilon_\infty\gamma^2}{\varepsilon_\infty}} \tag{4}$$

$$\epsilon(\omega) = \epsilon_\infty - \frac{\omega_p^2}{\omega^2 + i\gamma\omega} \tag{5}$$

where $\epsilon_\infty$ is the high frequency permittivity, $\omega$ is the angular frequency, and $\gamma$ is the electron scattering rate.

$$\mu = \frac{e\tau}{m_e} \tag{6}$$

By electrostatic modulating $N(z)$, the local plasma frequency $\omega_p(z)$ is altered, thereby shifting the ENZ condition $[Re\{\epsilon(\omega)\} \approx 0]$ (4) and consequently changing optical response of the material. Application of voltage biasing leads to a change in mobility $\mu$ which in turn alters $\gamma$ as per (6).

Thick bottom Ag substrate ensures negligible transmission thus ensuring A = 1-R where A and R denote absorption and reflection respectively. The equations used to compute R using TMM is given as:

$$R = |r|^2 = \left|\frac{M_{21}}{M_{11}}\right|^2, \tag{7}$$

where $M_{11}$ and $M_{21}$ are the elements of the Overall Transfer Matrix $M$ [11]:

$$M = \begin{bmatrix} M_{11} & M_{12} \\ M_{21} & M_{22} \end{bmatrix}$$

## IV. RESULTS AND DISCUSSION

On application of electrical potential of 15V to the bottom Ag layer, the electron concentration at the semiconductor insulator interface reaches approximately $10^{22}$ at the semiconductor insulator interface and then exponentially declines along the height of the semiconductor eventually reaching a saturation value of $3.5 \times 10^{17}$ near the upper edge of semiconductor layer (Fig.2). This leads to accumulation of majority charge carriers near the insulator interface. As evident from Fig.3, a fraction of the total external voltage suffers a drop across the semiconductor layer.

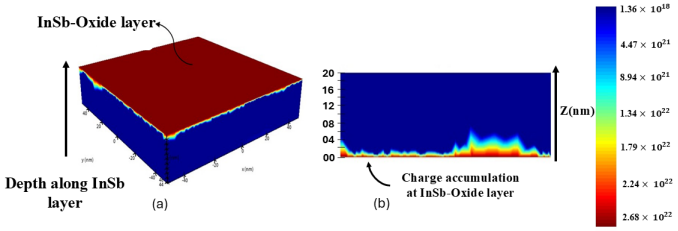


Fig. 2. (a):3D plot of carrier concentration distribution (N) along the depth of n-InSb layer in Al-InSb-$HfO_2$-Ag structure when Electrical gating of 15 V is applied (b):YZ plot of Carrier Concentration distribution (N) along the height of n-InSb layer in Al-InSb-$HfO_2$-Ag structure when Electrical gating of 15 V is applied, where z = 0 denotes Al-InSb interface.

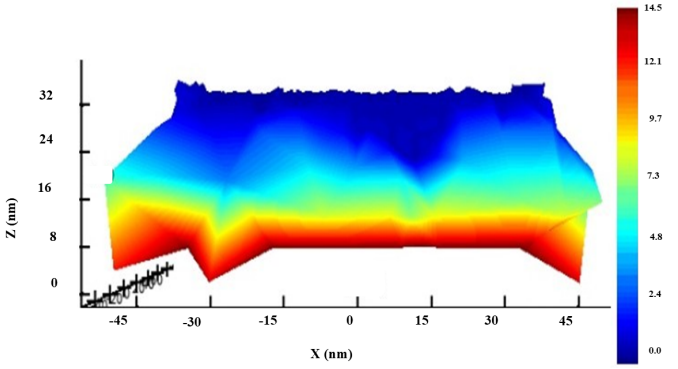


Fig. 3. 3D plot for electric potential distribution (V) along cavity region (InSb-insulator) for Al-InSb-$HfO_2$-Ag structure when electrical gating of 15 V is applied , where z = 0 denotes Ag-$HfO_2$ interface.

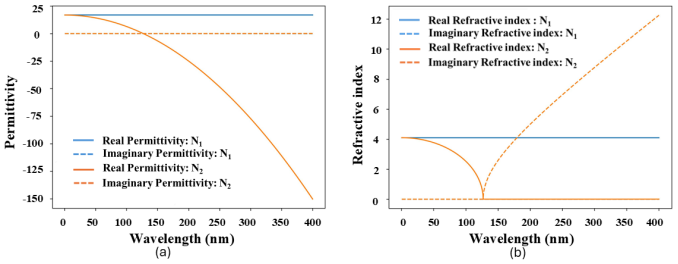


Fig. 4. (a): Permittivity plot for n-InSb where $N_1 = 3.5 \times 10^{17}\,\mathrm{cm}^{-3}$ and $N_2 = 2.68 \times 10^{22}\,\mathrm{cm}^{-3}$. (b): Refractive Index plot for n-InSb where $N_1 = 3.5 \times 10^{17}\,\mathrm{cm}^{-3}$ and $N_2 = 2.68 \times 10^{22}\,\mathrm{cm}^{-3}$.

As depicted from Fig.4, with application of voltage bias, there is a shift of ENZ wavelength to 126 nm. The alteration is governed by the Drude dispersion model as $\omega_p$ and $\gamma$ become altered with change in carrier concentration from $N_1$ to $N_2$. This leads to an overall modification of the optical response of InSb.

Figure 5 compares the reflectance spectra of three nanostructures using TMM. The $ZrO_2$ and $HfO_2$ cases show nearly identical resonant wavelengths, while $TiO_2$ exhibits a slight deviation. At 0 V bias, the resonances occur at 495 nm, 520 nm, and 505 nm for structures (a), (b), and (c) respectively, along with an approximately 95.8 % change in reflectance, transforming the device from highly reflective to perfectly absorbing. Under 15V bias, they shift to 455 nm, 485 nm,

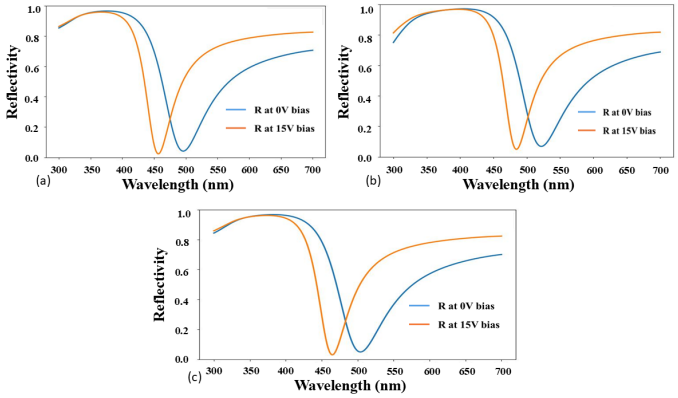


Fig. 5. Reflectance spectra plots for (a): Al(10nm)-InSb(20nm)-**$HfO_2$(15nm)**-Ag(100nm). (b):Al(10nm)-InSb(20nm)-**$TiO_2$(15nm)**-Ag(100nm). (c): Al(10nm)-InSb(20nm)-**$ZrO_2$(15nm)**-Ag(100nm).

and 470 nm, corresponding to blue shifts of 40 nm, 35 nm, and 35 nm. A modest increase in reflection dip upto 97.6% is also observed under 15V bias, enhancing their behavior as selective light absorbers.

To further probe the effect of the insulator, the cavity thickness was increased (semiconductor from 20 nm to 50 nm, insulator from 15 nm to 100 nm). TMM analysis of these modified structures highlights the role of cavity scaling in tailoring optical response.

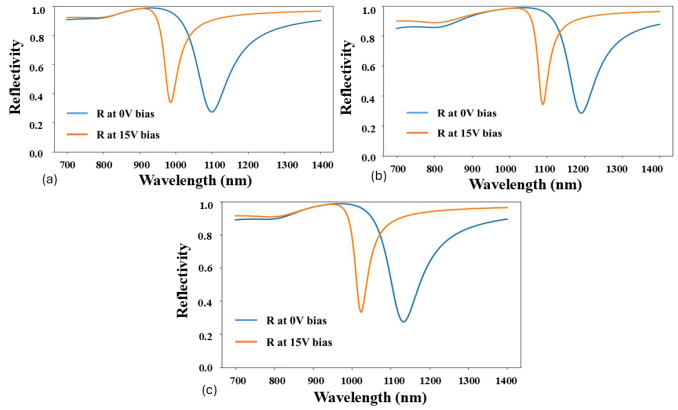


Fig. 6. Reflectance spectra plots for (a): Al(15nm)-InSb(50nm)-**$HfO_2$(100nm)**-Ag(100nm). (b):Al(15nm)-InSb(50nm)-**$TiO_2$(100nm)**-Ag(100nm). (c): Al(15nm)-InSb(50nm)-**$ZrO_2$(100nm)**-Ag(100nm).

As depicted by Fig.6, there is a redshift of resonant wavelength to the near infrared region. A significant contrast is noted among the optical responses of the insulating materials. Within the altered thickness nanocavities investigated, InSb-$TiO_2$ nanostructure exhibits the greatest redshift in resonant wavelength for 0V condition which is computed to be 1.19 $\mu$m. InSb-$HfO_2$ and InSb-$ZrO_2$ cavity nanostructures exhibit resonant wavelengths of 1.1 $\mu$m and 1.13 $\mu$m for the 0V biasing condition. The observed contrast can be attributed to the different refractive index properties for the different insulator medium, which was not significant in the nanocavity previously studied with a semiconductor-insulator thickness of

20nm-15nm as the insulator thickness was too less compared to the nanocavity thickness to exhibit such behavior. There is also a significant increase in spectral blue shift on applying electrical bias of 15V. The observed values for electrically tuned spectral shift are: 115 nm , 100 nm and 105 nm for structures (a) , (b) and (c) respectively. However, the reflectance dip falls to 73.7 % , thus rendering the structure comparatively less suitable for selective absorption based operations.

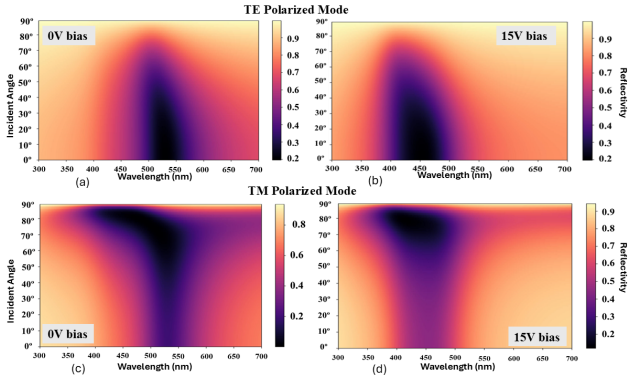


Fig. 7. (a) and (b) : TE polarized plots for 0V and 15V respectively for Al(10nm)-InSb(20nm)-$ZrO_2$(15nm)-Ag(100nm) (c) and (d) : TE polarized plots for 0V and 15V respectively for Al(10nm)-InSb(20nm)-$ZrO_2$(15nm)-Ag(100nm).

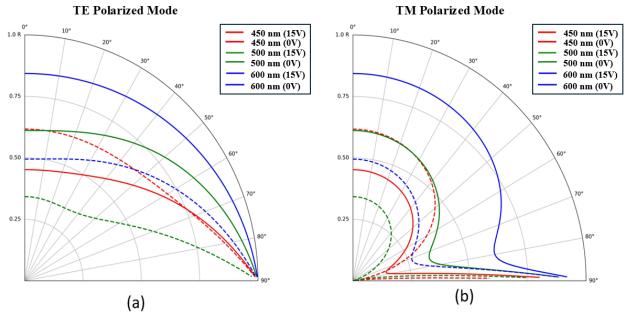


Fig. 8. (a): Reflectance Polar plot for TE mode (b); Reflectance polar plot for TM mode; in Al(10nm)-InSb(20nm)-$ZrO_2$(15nm)-Ag(100nm).

Next we take the InSb(20 nm)-$ZrO_2$(15 nm) nanostructure and perform Transverse Electric (TE) and Transverse Magnetic (TM) polarized TMM calculations, varying the angle of incidence from 0 to 90 degrees in the visible range. Fig.7 shows the angle resolved reflectance colormap in the visible region obtained for TE and TM polarized modes at 0V and 15V biasing conditions for the same structure. As expected, the electrical spectral shift is clearly evident in either case. The reflectance vs angle of incidence polar plot for the same structure exhibits a similar trend for chosen wavelengths of 450 nm, 500nm and 600 nm. One interesting feature is that the reflectance computed in TE mode is relatively insensitive to the angle of incidence as compared to that in TM mode which drops to a sharp and distinct minimum at a specific angle before rising steeply towards total reflection at 90°. This angle of minimum reflectance is the pseudo-Brewster's angle for that specific wavelength and bias condition.

## V. CONCLUSION

In this paper, we have shown numerically the operation of an electrically tunable selective light absorber based on an Fabry-Perot nanocavity using n-doped InSb as an active medium that exhibits ENZ characteristics. By coupling electrostatic simulations with optical modeling, we demonstrated the ability to tune through the ENZ wavelength of InSb with electrical gating, enabling the first observation of displacement current generated dynamic shift of peak absorption wavelength in the visible region. A comparison using $TiO_2$, $HfO_2$, and $ZrO_2$ as gate dielectrics illustrated the importance of high-k oxide selection to increase reflectance dip, while the cavity thickness engineering, allowed us to extend that resonance from the visible into the near-infrared. The proposed device achieves a maximum spectral shift of 40 nm in the visible region with a reflectance dip of 97.6%, and a 115 nm shift in the near-infrared region with a dip of 73.7% for the $HfO_2$-based nanostructure. Overall, these results provide a potential pathway to compact, CMOS-compatible, and dynamically tunable light absorbers for the next generation of photonic and optoelectronic device.

## REFERENCES


[1] L. C. Kimerling et al., "Electronic-photonic integrated circuits on the CMOS platform," presented at the Integrated Optoelectronic Devices 2006, J. A. Kubby and G. T. Reed, Eds., San Jose, CA, Feb. 2006, p. 612502. doi: 10.1117/12.654455.

[2] C. Gunn, "CMOS Photonics for High-Speed Interconnects," IEEE Micro, vol. 26, no. 2, pp. 58–66, Mar. 2006, doi: 10.1109/MM.2006.32

[3] C. Gutierrez-Martinez, G. Trinidad-Garcia, and J. Rodriguez-Asomoza, "Electric field sensing system using coherence modulation of light," IEEE Trans. Instrum. Meas., vol. 51, no. 5, pp. 985–989, Oct. 2002, doi: 10.1109/TIM.2002.806017

[4] M. Z. Yaqoob, M. Ahamd, A. Ghaffar, F. Razzaz, S. M. Saeed, and T. M. Alanazi, "Thermally tunable electromagnetic surface waves supported by graphene loaded indium antimonide (InSb) interface," Sci. Rep., vol. 13, no. 1, p. 18631, Oct. 2023, doi: 10.1038/s41598-023-45475-8

[5] T. S. Moss, S. D. Smith, and T. D. F. Hawkins, "Absorption and Dispersion of Indium Antimonide," Proc. Phys. Soc. Sect. B, vol. 70, no. 8, pp. 776–784, Aug. 1957, doi: 10.1088/0370-1301/70/8/307.

[6] C. K. Maiti, G. K. Dalapati, S. Chatterjee, S. K. Samanta, S. Varma, and S. Patil, "Electrical properties of high permittivity ZrO2 gate dielectrics on strained-Si," Solid-State Electron., vol. 48, no. 12, pp. 2235–2241, Dec. 2004, doi: 10.1016/j.sse.2004.04.012.

[7] Ansys Lumerical, Charge Solver: https://optics.ansys.com/hc/en-us/articles/360034917693-CHARGE-solver-introduction

[8] Palik, E. D. Handbook of Optical Constants of Solids (Academic Press, 1985).

[9] Dixit, K.P., Gregory, D.A. Nanoscale modeling of dynamically tunable planar optical absorbers utilizing InAs and InSb in metal-oxide-semiconductor–metal configurations. Discover Nano 18, 100 (2023). https://doi.org/10.1186/s11671-023-03879-5

[10] Mohamed Ellio, Franlin Che, Michael Cada; "Drude-Lorentz Model of Semiconductor Optical Plasmons: ; January 2014 ; doi : http://dx.doi.org/10.1007/978-94-007-6818-5-4

[11] Tom G. Mackay, Akhlesh Lakhtakia ; The Transfer-Matrix Method in Electromagnetics and Optics ; April 2020 ; DOI: 10.2200/S00993ED1V01Y202002EMA001